







MyoBio: An Automated Bioreactor System Technology for Standardized Perfusion-Decellularization of Whole Skeletal Muscle

Paul Ritter , Aijia Cai , Barbara Reischl, Maren Fiedler, Gerhard Prölb, Benjamin Frieß, Elke Kretschmar, Mena Michael , Kristin Hartmann, Christian Lesko, Haitham Salti, Andreas Arkudas, Raymund Horch, Friedrich Paulsen , Oliver Friedrich , and Michael Haug 

Abstract—Objective: Decellularizing solid organs is a promising top-down process to produce acellular bioscaffolds for ‘de novo’ regrowth or application as tissue ‘patches’ that compensate, e.g., large volumetric muscle loss in reconstructive surgery. Therefore, generating standardized acellular muscle scaffolds marks a pressing area of need. Although animal muscle decellularization protocols were established, those are mostly manually performed and lack defined bioreactor environments and metrologies to assess decellularization quality in real-time. To close this gap, we engineered an automated bioreactor system to provide chemical decellularization solutions to immersed whole rat *gastrocnemius medialis* muscle through perfusion of the main feeding arteries. **Results:** Perfusion control is adjustable according to decellularization quality feedback. This was assessed both

from (i) *ex situ* assessment of sarcomeres/nuclei through multiphoton fluorescence and label-free Second Harmonic Generation microscopy and DNA quantification, along with (ii) *in situ* within the bioreactor environment assessment of the sample’s passive mechanical elasticity. **Conclusion:** We find DNA and sarcomere-free constructs after 72 h of 0.1% SDS perfusion-decellularization. Furthermore, passive elasticity can be implemented as additional online decellularization quality measure, noting a threefold elasticity decrease in acellular constructs. **Significance:** Our *MyoBio* represents a novel and useful automated bioreactor environment for standardized and controlled generation of acellular whole muscle scaffolds as a valuable source for regenerative medicine.

Index Terms—Biomechatronics, bioreactors, tissue engineering, decellularization, skeletal muscle.

I. INTRODUCTION

PATIENTS suffering from irreversible muscle loss, either due to trauma, necrosis or tumor ablation, currently exclusively rely on the use of autologous muscle grafts (involving, e.g., *M. gracilis*, *M. latissimus dorsi*) [1], which often leads to impaired functional recovery and reduced motility/strength even after prolonged physical rehabilitation [2], [3]. Unfortunately, more than 10% of all reconstructive surgeries eventually fail due to graft infection [4], and are also accompanied by the risk of donor site morbidity [2]. To overcome such limitations of autologous transpositions [1], [2], [5], new methods in tissue engineering aim to find sustainable alternatives for heterologous transplantation approaches [6]–[8]. In that regard, a promising approach is the bio-engineering of organs via tissue-printing (bottom-up), [9]–[11] or the recreation of acellular scaffolds that serve as either meshwork to re-engineer organs from patient recipient cells (top-down) [12], or for direct implantation as biomimetic ‘muscle tissue patch’ to enhance muscle regeneration [13], [14]. Particularly, the top-down approach to obtain bio-scaffolds from previously intact organs reflects a promising method as it conserves the vascular network and the specific tissue-inherent architecture which is usually challenging to achieve in bio-printing and has not yet been convincingly demonstrated in bottom-up processes [15]–[17].

Manuscript received April 12, 2021; revised October 22, 2021; accepted January 4, 2022. Date of publication January 13, 2022; date of current version June 20, 2022. The work of Oliver Friedrich and Michael Haug were supported by the Central Innovation Program SME of the German Ministry of Economics and Technology ZIM-Kooperationsprojekt under Grant ZF4134307CR08, the work of Paul Ritter and Oliver Friedrich were supported by the Erlangen Graduate School in Advanced Optical Technologies (SAOT, Graduate School GSC 80, Deutsche Forschungsgemeinschaft), the work of Oliver Friedrich and Raymund Horch were supported by the Deutsche Forschungsgemeinschaft (DFG, German Research Foundation) under Project Number 326998133 TRR 225 Biofabrication (subproject B08 and subproject C04), and the work of Friedrich Paulsen was supported by DFG Project under Grant PA738/15-1. (Paul Ritter and Aijia Cai contributed equally to this work.) (Michael Haug and Oliver Friedrich are senior co-authors.) (Corresponding author: Paul Ritter.)

Paul Ritter is with the Institute of Medical Biotechnology, Friedrich-Alexander-University Erlangen-Nürnberg, 91052 Erlangen, Germany (e-mail: paul.p.ritter@fau.de).

Aijia Cai, Benjamin Frieß, and Andreas Arkudas are with the Plastic and Hand Surgery, Universitätsklinikum Erlangen, Germany.

Barbara Reischl, Maren Fiedler, Gerhard Prölb, Mena Michael, Kristin Hartmann, Christian Lesko, Raymund Horch, Oliver Friedrich, and Michael Haug are with the Institute of Medical Biotechnology, Friedrich-Alexander-University Erlangen-Nürnberg, Germany.

Elke Kretschmar and Friedrich Paulsen are with the Institute of Functional and Clinical Anatomy, Friedrich-Alexander-University Erlangen-Nürnberg, Germany.

Haitham Salti is with the Department of Extracorporeal Immunomodulation, Fraunhofer Institute for Cell Therapy and Immunology (IZI), Germany.

Digital Object Identifier 10.1109/TBME.2022.3142317

The technical proof-of-concept and validity of recreating artificial organs using this technique has already succeeded in initial studies for heart [18], [19], liver [20], and lung in a confined lab environment [21]. However, the methodological translation to skeletal muscle has proven difficult due to the strict and highly conserved structure of serially aligned repetitions of actin and myosin in sarcomeres as well as the parallel alignment of myofibrils that form a single muscle cell. Reconstructing an organ of such delicate structural hierarchy not only requires precise control over environmental parameters but also demands mechano-electrical preconditioning during regrowth. Moreover, also during the process of decellularization, the muscle needs to be kept under sustained passive mechanical strain. For instance, a muscle detached from tendons without imposed mechanical strain only survives for a very limited time as muscle cells will shorten and integrity will be irreversibly diminished [22], [23]. Although researchers have already made striking advancements in recreating functional skeletal muscle in rat forearms [24], the aforementioned challenges still represent a bottleneck for long-term viability studies. Consequently, clinicians currently rather rely on implanting biomimicking muscle scaffolds [7], [25], or acellular extracellular matrix (ECM) scaffolds, which enhance the natural repair mechanisms in patients and thus, represent a promising approach to sustainably treat volumetric muscle loss (VML) [13], [14]. Unfortunately, the methodology to obtain these scaffolds remains labor-intensive and depends on individual experience [6], [24]. This prevents ECM muscle scaffolds to be used routinely in reconstructive surgery and points towards a general need for automation and standardization.

In this study, we present a novel engineered bioreactor system (*MyoBio*, Fig. 1(A)) that allows the autonomous generation of standardized acellular muscle scaffolds with robust quality output. The system is designed to facilitate and automate the process of tissue decellularization and is not restricted to solute diffusion barriers in an unstirred layer that normally limits immersion-decellularization techniques to a tissue depth of approx. 200 μm [20]. The *MyoBio* tackles this challenge by rather applying a perfusion-decellularization approach, combining two perfusion circuits in a perfusion bioreactor system. In addition to a continuous detergent exchange of the bioreactor chamber, the decellularizing solution is also applied to within the deep tissue via cannulation of the arterial feed branch, in our case the popliteal artery of the isolated *gastrocnemius* muscle. While constantly flushing the medial head of the *gastrocnemius* muscle from inside and outside with decellularizing detergent (0.1% sodium dodecyl sulfate (SDS) (w/v)), the *MyoBio* tracks the sample's passive elastic properties in resting length-tension (RLT) curves over the time course of decellularization (here: 72 h). A serial dilution of decellularizing SDS detergent allowed us to determine the most suitable concentration for a balanced trade-off between decellularization time and efficacy. We compared the differences between diffusion- and perfusion-decellularization, assessing the quality of the ECM scaffold with label-free multiphoton Second Harmonic Generation microscopy and DNA quantification assays. Lastly, we also investigated the possible effects of mechanical actuation during decellularization. The series of experiments confirm the suitability

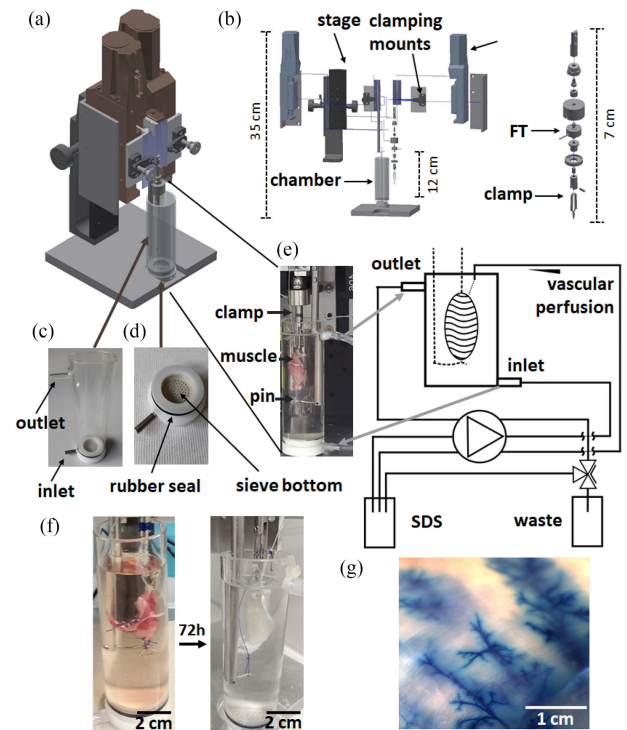


Fig. 1. *MyoBio* system setup and flow chart for automated muscle decellularization. (a) CAD construction drawing of the *MyoBio* bioreactor with its key components highlighted and named in the (b) explosion drawing to the right. (c) and (d) display an enhanced view of the reactor chamber and the sealing sieve bottom. (e) shows a photograph of a clamped muscle sample in the reactor chamber during system operation. A flow chart of the system is given to the right. The reactor is either operated in continuous flow mode for perfusion-decellularization (valve directs to SDS) or in batch mode (valve directs to waste) for future cell re-seeding experiments. A hose pump flushes the system with 0.1% SDS (w/v) in ddH₂O through both, the chamber inlet and the muscle's vasculature. In perfusion or loop configuration, the SDS reservoir also serves as a waste flow. (f) After 72 h, the muscle has predominantly lost its myoglobin and presents translucent. (g) Flushing the vasculature with methylene blue confirmed the integrity of the vascular system within the isolated muscle.

of our *MyoBio* bioreactor to act as a vanguard model towards autonomous and standardized processing of native skeletal into muscle ECM scaffolds that could accelerate their routinized application in reconstructive surgery.

II. MATERIAL AND METHODS

A. *MyoBio* Bioreactor System

1) **Hardware Components:** The *MyoBio* bioreactor system (Fig. 1(A)) is designed to meet the demands of a fully automated platform to create acellular skeletal muscle ECM scaffolds which may be further used as muscle patches in transplantation medicine or as a precursor for recellularization bioprocess optimization. The system is composed of two linear motors (L-406, Physik Instrumente (PI) GmbH & Co. KG, Karlsruhe, Germany) that allow to adjust the prestretch to the length of each individual muscle and to perform mechanical stimulation and biomechanical characterization of the sample during decellularization. Each motor spans an actuation range of 25 mm, allowing a maximum

of 50 mm stretch/actuation. Both motors are connected to a manual Z-stage for initial height adjustment. Spring fastening clamping mounts were installed to facilitate pin attach- and detachment to simplify sample mounting and transportation. One of these pins is composed of a force transducer (8411, burster, GmbH & Co. KG, Gernsbach, Germany, $F_{max} = 10$ N) in series with a bulldog clamp to which the proximal tendon of the sample muscle (*M. gastrocnemius medialis*) is attached. The other pin features a rod with a notch to fix the distal tendon (Fig. 1(B)). A central feature of the *MyoBio* is a glass cylinder that forms the reactor chamber (Fig. 1(C)). It is composed of a detachable sieve bottom which is sealed with a Teflon ring (Fig. 1(D)). The sieve bottom represents the fluid inlet and increases fluid dispersion. The outlet connector is located at the top of the glass cylinder (Fig. 1(C)). The entire composite of a mounted muscle in the reactor chamber is illustrated in Fig. 1(E) which also governs the system in two independent perfusion circuits. The first fluidics circuit (pump channel 1) constantly supplies the reactor chamber with decellularizing detergent (SDS at 7.5 ml min^{-1}). After completion of decellularization, the reactor chamber is washed with dH₂O with a flow speed of 11.8 ml min^{-1} for 21 min. The second fluidics circuit flushes the deep tissue of the muscle organ through its vascular cannulation at 1.2 ml min^{-1} . Both fluidics circuits are digitally controlled by a 4-channel hose pump (Reglo ICC Digital, Ismatec Cole Parmer GmbH, Wertheim, Germany). In addition, a manually operated three-way valve allows switching between continuous and batch-flow operation. The entire perfusion-decellularization process was optimized for 72 h and conducted at RT (Fig. 1(F)).

2) Software and Systems Electronics: Both linear actuators are connected in a daisy chain configuration to the C-863 Mercury Servo Controller (Physik Instrumente (PI)) and transmit serial data via USB to the CPU. The entire control software was written in C and Python which also governs reading out FT data. A custom-made GUI allows controlling the motors manually before mounting and to set up different biomechanical stretch stimuli to execute during the decellularization protocol. Various biomechanical stimulation or testing methods can be chosen from, with a wide range of additional adjustments, like wave-form stimuli (e.g. saw-tooth wave, sine wave, etc.), conditionals (stop at a certain tissue compliance, at a maximum/minimum passive restoration force or at a defined time-point), biomechanical testing methods (RLT-curves, etc.), methods with force-feedback dependence or other methods important for user-handling (bug-fix mode, pause, end methods, etc.). Furthermore, the flow-rate and fluid direction of the hose pump is also controlled via the GUI.

B. Animal Model and Muscle Preparation

Donor animals were male Lewis rats (*rattus norvegicus*) of ca. 300 g weight. Anesthesia was induced by inhalation of 4% isoflurane under spontaneous breathing with butarphenol and meloxicam as an analgetic. All animal procedures were performed in accordance to the German regulations for the care of laboratory animals at all times. Experiments were approved by the local animal care committee and government (approval

number: 55.2.2-2532.2-658-48). Rats were in supine position and *gastrocnemius* muscle was prepared through an incision on the anterior hind limb. Adductor muscles were dissected to expose *gastrocnemius* muscle with its insertions at the femur (proximal) and the achilles tendon (distal). All feeding vessels except for the popliteal artery and vein as the main pedicle of the *gastrocnemius* muscle were ligated. The medial head of the *gastrocnemius* was dissected from the lateral head and the proximal and distal insertions were detached from the femur and the achilles tendon, respectively. The femoral artery was cannulated via a polyethylene catheter (0.28 mm diameter, Smiths medical, Grasbrunn, Germany) which was connected to a cannula to ensure intraarterial perfusion. All vessels branching off the femoral artery and vein except for the popliteal vessels were ligated. The femoral artery and vein were dissected proximally from the catheter and the muscle including its (cannulated) pedicle was completely freed and taken for further processing. Rats were sacrificed after the procedure. The bulldog clamp was detached from the *MyoBio* and clamped to the proximal tendon of the *M. gastrocnemius medialis*, while the distal end was tied to a loop of surgical thread. Ensuring not to damage the vascular cannulation, the clamp and muscle were transferred to the reactor chamber filled with SDS, and the clamp was re-attached to the linear actuator. The distal end of the muscle was fixed by slipping the thread loop over a pin with a notch. Finally, the vascular cannulation was connected to the fluidics system, allowing pump-driven perfusion decellularization.

C. Biomechanical Assessment During Perfusion-Decellularization

During perfusion-decellularization with 0.1% SDS (w/v) for approx. 72 h, RLT-recordings were carried out to monitor the change in passive elasticity while the muscle was continuously freed of its cellular components. To contrast these changes, we conducted RLT assessments to stretch the preparation up to 115% of its resting length at a velocity of $2 \mu\text{m s}^{-1}$ which is close to the quasi-static stretch regime.

Since the muscle length is subject to change during the decellularization process, the initial restoration force was set to 70 mN to define the initial resting length L_0 before and after decellularization. The force-time data were stored as a text file for subsequent analysis. Along with the development of the *MyoBio*, we also implemented automated analysis algorithms for data evaluation. After extracting the force-time data and transforming them to a force-length relation, maximum restoration force was derived at 115% L_0 . A linear fit was applied to each section of 5% stretch, using least-square method, and compliance was calculated based on the inverse of that slope. Data were plotted as box plots in Origin 2019 (OriginLab Corporation, Northampton, Massachusetts, USA). One-Way ANOVA testing was performed followed by post-hoc Bonferroni analysis.

D. Optical Clearing

The muscle (either native or decellularized) was pinned onto a silicone-elastomer-coated Petri dish (Sylgard, Dow Corning,

Midland, Michigan, USA) and immersed in 4% paraformaldehyde (PFA). The composite was then placed on a shaker for 2 h at 30 rpm at room temperature (RT). To subsequently clear the muscle sample, it was immersed in 10 ml of increasing 2,2-Thiodiethanol (TDE) concentrations (volume fractions used: 30%, 50%, 70%, and 80%) [45]. Each step was performed for 4 h on a shaker at 30 rpm at RT. Samples were stored in 80% TDE at 4 °C overnight.

E. Two-Photon Second Harmonic Generation Microscopy

A multiphoton system (TriM-scope II; LaVision BioTec GmbH; Bielefeld) with a femtosecond pulsed Ti:Sa laser was used to image muscle samples (water immersion objective (25x Zeiss, Jena, Germany)) for myosin-II and collagen-I structures. The Ti:Sa laser was tuned to a wavelength of 810 nm to simultaneously excite both proteins. A photomultiplier was used with a band-pass filter at 405 nm \pm 10 nm. Images were acquired with a total resolution of 1,024 x 1,024 or 512 x 512 pixels, respectively. Images were processed in Image J (National Institute of Health, Bethesda, Maryland, USA) to apply gamma correction, adjusted brightness for enhanced visualization, and further colorization with a red & blue lookup-table.

F. Scanning Electron Microscopy

Microscopy slides were silanized in a custom-manufactured 3D slide holder made of polytetrafluorethylene. Before treatment, all microscopy slides were cleaned for 10 min in pure isopropanol (100%) to minimize artifacts during SEM imaging. Subsequently, the slides were incubated in 2% (3-Aminopropyl)triethoxysilane (APTES) for 10 min and further treated with pure acetone (100%) twice. Furthermore, the slides were washed thrice with millipore water for 10 min each and dried for a minimum of 24 h before further use. SEM imaging was performed with the JSM-IT300LV electron microscope (Jeol Ltd, Tokyo, Japan) at a low vacuum. Muscle cryosections were collected on silanized 20 mm x 20 mm microscopy slides, coated with indium tin oxide (ITO) and washed with a solution of 1% osmium in 0.1 M cacodylate buffer (1:1) for 2 h. Dehydrating the samples was performed with an ascending alcohol series, followed by further treatment with acetone, before drying them in a critical point dryer (Leica EM CPD 300, Wetzlar Germany). Finally, the samples were spotted with gold particles in a low vacuum coater (Leica EM ACE 200, Wetzlar Germany). Images received no further adjustments.

G. DNA Quantification

A genomic DNA purification kit (GeneJet) from Thermo Scientific (Waltham, MA, USA) was used to extract genomic DNA from native and decellularized muscle samples, from the surface and the deep tissue. Purity of the isolated genomic DNA was confirmed via optical absorbance spectroscopy by

calculating the ratio of $\frac{Abs_{260}}{Abs_{280}}$. Finally, the DNA was quantified with a Nanodrop 2000 (Thermo Scientific, Waltham, MA, USA).

III. RESULTS

The engineering of an automated bioreactor system to create cell-free muscle scaffolds required a highly established decellularization technique, which allows system validation with an easily executable protocol. As such, the chosen decellularization method (0.1% SDS in ultra-pure water for 72 h) satisfied the ease-of-use criterion and yielded a better scaffold quality as compared to other decellularization techniques in skeletal muscle tissue (data not shown). For an adequate validation, our *MyoBio* was applied to decellularize *gastrocnemius medialis* muscle over 72 h of automated system operation.

A. Critical Bioreactor Improvements Stabilized the Decellularization Process

Initial experiments revealed the importance of a centralized and stable positioning of the perfusion tube to allow a strain-relieved perfusion. With the loss of structural proteins inside of the vascular system, already small vertical or horizontal forces were enough to lose the vascular tubing and lead to the inevitable abortion of the experiment. This was especially critical during biomechanical experiments. Additionally, flow speeds were optimized by tracer experiments to minimize dead volume inside of the reactor chamber while having an acceptable volume exchange to remove cellular debris effectively. The volume flow to flush deep tissue of the muscle was gradually decreased to 1.2 ml min⁻¹ until stability of the system, both during biomechanical experiments, as well as during perfusion-decellularization was ensured. Higher speeds led to external vascular rupture and scaffold swelling. The washing time was optimized via residence time experiments to 21 min which is three times the time that is needed to displace 95% of the total volume to ensure the full removal of SDS and cellular debris in the bioreactor vessel. Further, since we wanted to ensure a constant flow regime at the muscle surface to allow optimal decellularization, we flipped the bioreactor inlet to the sieve bottom. As a beneficial side effect, it allowed us to more easily control the total fluid volume by removing the excess fluid volume at the bioreactor outlet.

B. 0.1% SDS Automated Perfusion-Decellularization Achieved a Profound Loss of Cellular Components

Initial decellularization experiments were conducted to identify an easy-to-use decellularization protocol in conjunction with our *MyoBio* bioreactor. Literature research yielded two promising approaches that were suitable in conjunction with an automated decellularization protocol, namely (i) osmotic shock and (ii) SDS decellularization [26], [27]. Each method was tested in a 72 h perfusion-decellularization experiment.

Fig. 2 displays Second Harmonic Generation images to compare native muscle to osmotic shock and SDS decellularized muscle scaffolds. Native muscle tissue (Fig. 2(A)) showed highly organized and repetitive sarcomeres, which were less

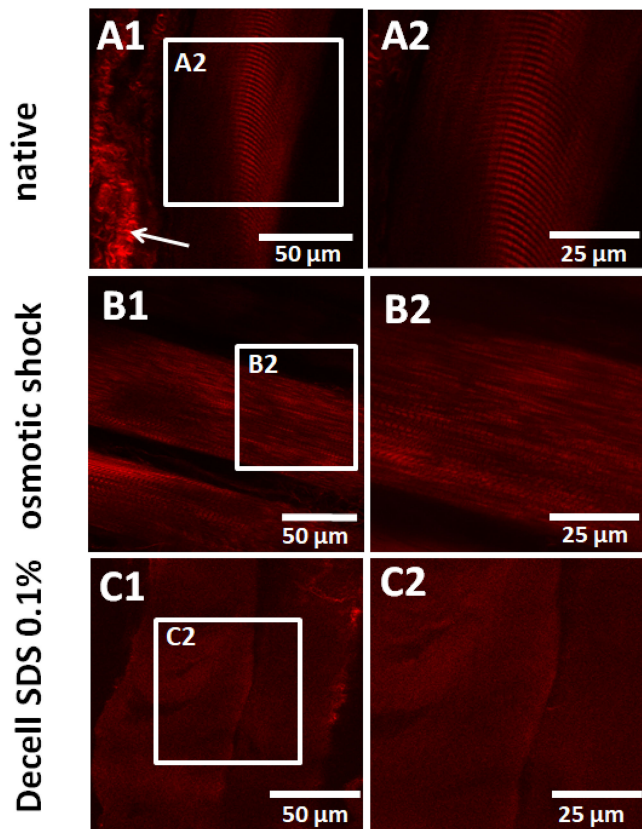


Fig. 2. SHG imaging confirms the absence of sarcomeres in *M. gastrocnemius medialis* after 72 h of 0.1% SDS perfusion-decellularization, while osmotic shock does not remove myofibrillar lattice components. (a) shows representative SHG images of a native *M. gastrocnemius medialis* single muscle fiber within the muscle with a highly organized sarcomere striation pattern. Closely entwined collagen-I fibers are marked with an arrow. (b) Osmotic shock, induced with ultrapure water in whole muscles, only caused swelling of cells and disrupted the regular arrangement of sarcomeres but preserved their SHG signal. (c) In contrast, sarcomere structure entirely vanished after three days of dual perfusion-decellularization with 0.1% SDS in ddH₂O water and was, except for minor protein residues, undetectable even at higher magnification, confirming successful decellularization.

pronounced in osmotic shock-treated muscle (Fig. 2(B)) and virtually absent in SDS decellularized muscle (Fig. 2(C)). Despite the remaining sarcomeric structure in osmotic shock-treated muscle samples, their myofibrils were out-of-register, leading to a disrupted myofibrillar arrangement. In contrast, when muscle tissue was decellularized with 0.1% SDS for 72 h, its sarcomere structure was profoundly absent.

Even though the initial decellularization experiment with 0.1% SDS yielded promising results, we sought to find the lowest possible concentration to adequately decellularize whole muscle tissue, since any remains of SDS could potentially compromise the bio-compatibility of the muscle scaffold. Therefore, we analyzed muscle samples that were decellularized at different SDS concentrations and subsequently treated with an optical clearing protocol. [45] This allowed us to image deep tissue segments (Fig. 3(A)) and verify their lack of cellular structural proteins, i.e. sarcomeric acto-myosin. Concentrations down to 0.05% and 0.075% SDS both showed incomplete

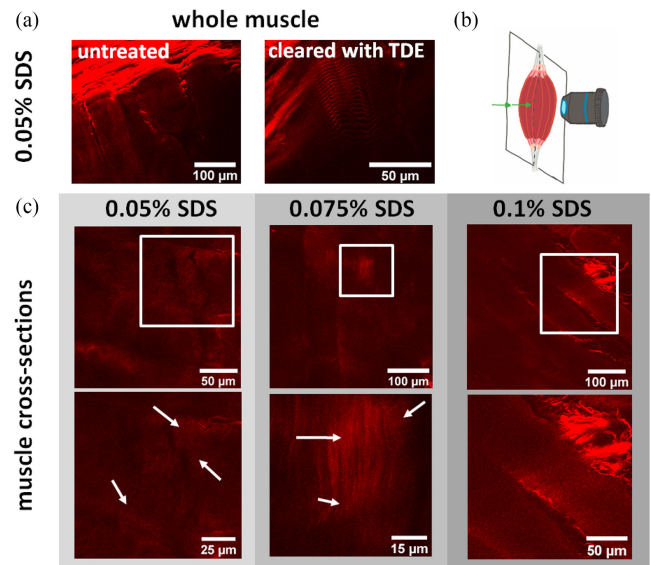


Fig. 3. SDS concentrations below 0.1% result in incomplete perfusion-decellularization within deeper tissue layers (~8 mm). (a) SHG signals of muscles treated with 0.05% SDS, imaged through whole muscle and optically cleared muscle, respectively. (b) For all samples shown here, we imaged the longitudinal cross-section with two photon microscopy of optically cleared samples. (c) After decellularization with 0.05% SDS, few intact sarcomeres remained visible within the deep tissue (arrows). When using 0.075% SDS, the sarcomere pattern still persisted after 72 h decellularization. Eventually, at 0.1% SDS, the decellularization protocol entirely cleared the tissue of cellular components.

decellularization in various locations of the muscle (Fig. 3(C)). This improved when advancing to a concentration of 0.1% SDS. Here, both deep tissue segments as well as the surface were completely decellularized (Fig. 3 A & C).

C. Microscopy Cross-Validation Confirms Protein Absence in Deep-Tissue Layers

To further confirm the quality of decellularized tissue, also (i) cross-validation with DAPI staining in combination with SHG myosin II imaging and (ii) scanning electron microscopy (SEM) was performed (Fig. 4 A & B). Both techniques independently show a loss of the muscle's native acto-myosin sarcomere structure, as well as the absence of cellular nuclei, and consequently align with our initial multiphoton-microscopy analysis.

D. Mechanical Stimulation Preserves Decellularization Quality

Another crucial quality parameter for successful decellularization is the quantity of remaining DNA per mg dry tissue (Fig. 4 C & D). A comparison between native and mere diffusion-decellularized tissue confirmed the latter to be inadequate for solid organ decellularization. Both samples did not differ significantly, neither when distinguished by probing surface- or deep tissue areas (Fig. 4 C), nor when comparing samples of different origin (Figure 4 D, native: ~ 150 ng mg⁻¹; diffusion-decellularized: ~ 140 ng mg⁻¹).

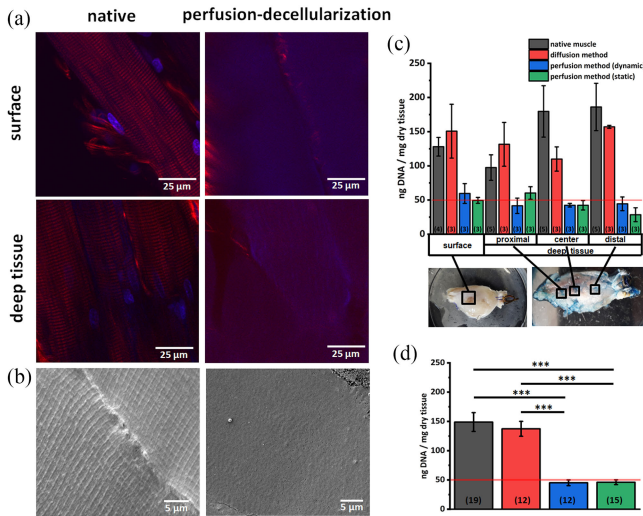


Fig. 4. Assessment of perfusion-decellularization quality confirms the loss of acto-myosin sarcomere structure. (a) SHG images comparing native to perfusion-decellularized muscle tissue after DAPI staining reveal a loss of sarcomere structure. (b) Electron-microscopy images of sarcomere ultra-structure show disorganization or vanishing of the native regular sarcomere pattern after decellularization. (c) DNA quantification of native, diffusion- and perfusion-decellularized muscle tissue extracted from the surface and deeper tissue. Regardless of whether using dynamic stretching or no stretch at all (static), perfusion-decellularization, in contrast to mere diffusion, thoroughly clears the whole muscle of its cellular content and falls below a limit of 50 ng DNA per 1 mg dry tissue. Numbers in round brackets correspond to the total sample size. (d) Combining surface and deep tissue samples statistically confirms the effectiveness of perfusion-decellularization. (***: $p < 0.001$).

Perfusion-decellularization, on the other hand, displayed significantly decreased DNA levels in comparison to native or diffusion-decellularized tissue and even fell below the suggested threshold of $\sim 50 \text{ ng mg}^{-1}$ DNA that indicates the scaffold to be considered ‘cell-free’ [28]. Here, we also compared a bio-mimicking perfusion-decellularization approach by dynamically stretching the muscle by 5% of its resting length (L_0) at a speed of 1 mm s^{-1} or not mechanically stimulating the sample at all. The corresponding static method revealed similar results ($\sim 46 \text{ ng mg}^{-1}$) as the dynamic method ($\sim 45 \text{ ng mg}^{-1}$) and mechanical stimulation reproduces decellularization quality.

To further ensure the complete decellularization of even deep tissue layers, we split the muscle horizontally (at approx. 8 mm depth) and sampled tissue segments at three different locations: proximal, central, and distal. Statistical analysis showed no significant difference between deep tissue segments and samples obtained from the surface of perfusion-decellularized muscle scaffolds, confirming a thorough decellularization through the vascular system.

E. Biomechanical Characterization Indicates a Reduction in Passive Axial Elasticity in ECM Scaffolds

Since we confirmed that mechanical actuation does not impede on the final scaffold quality (no difference in remaining DNA content detected), this indicated that we could implement online passive elasticity assessment in our automated *MyoBio*

decellularization protocol without inducing stretch-induced artifacts to the decellularization process. This allowed us to track the muscle’s passive axial elasticity in resting-length tension (RLT) force-strain curves. We stretched the muscle to a maximum of 115% L_0 to ensure that once decellularized, the muscle can still endure the assessment. The recorded RLT curves (Fig. 5(A) & (B)) confirmed our hypothesis of decreasing passive restoration force and revealed a loss between 30-50% in all initially tested muscles ($n=3$). Combined analysis of passive restoration force (Fig. 5(C)) revealed maximum force values of $\sim 0.35 \text{ N}$ for native muscle, which was reduced to $\sim 0.25 \text{ N}$ in decellularized scaffolds. To calculate the respective compliance from the RLT curve, it was further divided into three sections of 5% stretch each. While for both, native, and decellularized tissue, compliance remained somewhat constant with stretch (Fig. 5(D) & (E)), a direct comparison suggests decellularized muscle scaffolds to be overall more compliant than native muscle, which indicates a loss of cellular elastic components (e.g. F-actin cytoskeleton, acto-myosin lattice, etc.), to a higher degree than the loss of intracellular compliance components. Muscle length increase of 13% was observed after decellularization due to swelling (Fig. 5(F)). This effect was, however, not significant.

IV. DISCUSSION

A wide range of existing and established decellularization techniques include the use of acidic or alkaline detergents (ionic, non-ionic, and zwitterionic), sophisticated combinations of enzymatic agents, or sequential physical treatments (e.g., pH- or temperature-driven), which renders them unsuitable for automated standardization due to their labor-intensity or methodological complexity. Therefore, we aimed to identify and test an easy-to-use decellularization protocol that would neither harm the fluidics to an alteration of the tube network of the *MyoBio* bioreactor system, nor require a high amount of intermediate steps, such as frequently changing detergent solutions, altering environmental conditions or manually conditioning or transferring the sample during the procedure. Such processes would demand an ever-increasing complexity of the fluidics handling system, numerous feedback-control-loops in the software and precise control over a multitude of biological, and physical environment parameters. Hence, we excluded all enzyme-related and pH-driven decellularization techniques in conjunction with our automated *MyoBio* system and rather favored detergent decellularization techniques. Established detergent-based decellularization techniques either rely on 3-[(3-cholamidopropyl) dimethylammonio]-1-propanesulfonate (CHAPS), Triton X-100, SDS or sodium desoxycholate (SDC) [29]. Unfortunately, previous *in vitro* decellularization studies by Simsa *et al.* (2018) in blood vessels suggested Triton-X-100 protocols to require 4 - 11 days, whereas CHAPS-related protocols are composed of several different steps, including 0.1 M NaOH [30], which would, on the long term, damage the tubing material. A viable alternative was suggested by Urciuolo *et al.* (2018) who decellularized mice limbs with 0.25% SDS for 72 h and a subsequent washing step with deionized water for 48 h [14]. A similarly easy-to-use protocol was described in Perniconi *et al.* (2011)

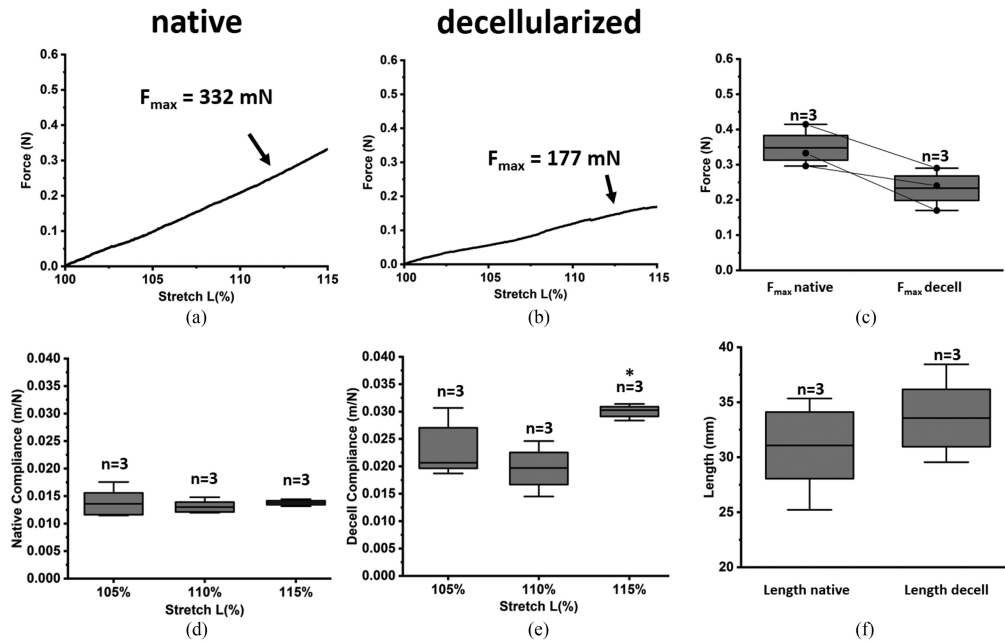


Fig. 5. Resting-length tension (RLT) curve of a perfusion-decellularized muscle shows an overall increase in compliance and decrease in elastic restoration force. RLT curves (a) before, and (b) after decellularization display a decline in passive restoration force (to ~30%) during decellularization in all tested muscles. (c) The combined maximum restoration forces (F_{max}) are quantified in a box plot. (d) While the overall compliance remains relatively constant with stretch in both native and (e) perfusion-decellularized muscle, the latter displayed a two-fold increase in overall compliance that indicates a partial loss of stiffness due to a loss of major elastic proteins (*: $p < 0.05$ decellularized vs. native muscle). (f) Total muscle length generally increased during decellularization (up to 13%) due to swelling (not significant). Stretch L(%) corresponds to passive elongation relative to the initial resting length.

who successfully decellularized a rat *extensor digitorum longus* muscle with 1% SDS for 24–48 h [26]. This protocol met the requirements of our automated *MyoBio* system and was further optimized towards utilizing the lowest SDS concentration possible since SDS alters the ECM and impedes on its property of promoting cell proliferation [31], [32], which would be essential for subsequent recellularization approaches. Therefore, we also compared the performance of osmotic shock decellularization which, due to the use of deionized water, represents a minimally invasive technique and preserves the proliferation-supporting properties of ECM. Unfortunately, apart from disrupting the myofibrillar alignment, osmotic shock did not sufficiently clear the muscle of its intracellular proteins, as demonstrated for myosin-II in Fig. 2(B). As such, we progressed with an SDS-based approach [29], and aimed at finding the lowest possible SDS concentration.

To further optimize our decellularization protocol for low SDS application, we conducted a morphological assessment after decellularization at different SDS weight to volume fractions (0.05%, 0.075%, and 0.1%) by performing SHG multi-photon microscopy (MPM) to label-free excite collagen-I and myosin-II. Fig. 2 (B1) & (B2) reveal the swelling and disruption of each muscle fiber. However, notable residues of myosin-II remained after a treatment of 72 h with ultra pure water. The application of 0.1% SDS led to the entire absence of myosin-II (Fig. 2(C)).

The samples of the serial SDS dilution were further checked with MPM for residues of sarcomeric patterns, as well as for DNA content (data not shown). Both, 0.05% and 0.075% SDS still revealed remains of myosin-II, and a corresponding DNA

content surpassing the threshold of 50 ng mg^{-1} DNA, as introduced by Crapo *et al.* (2011) [28]. Only the use of 0.1% SDS led to complete removal of cellular substances (Fig. 3(C)). Hence, we concluded that 0.1% is the optimal decellularization concentration to use with our *MyoBio* bioreactor system similar to a previous successful study [33]. However, Mayorca-Guiliani *et al.* (2019) used a manual perfusion-decellularization approach on whole mouse segments.

Since diffusion-based decellularization protocols were confirmed to be unsuitable for decellularizing solid organs, such as muscles (Fig. 4), we established perfusion-decellularization by cannulating the proximal branches of the popliteal artery feeding the *M. gastrocnemius medialis* and additionally supplying the deep-tissue parts with SDS through the intact intra-muscular vascular system. To also confirm the loss of intracellular proteins here, we performed cryosections of surface tissue and deep-tissue muscle layers (Fig. 4(B) & (D)) of both decellularized and native tissue. Subsequent staining of the samples with DAPI revealed that nuclei were absent in both surface and deep-tissue segments after perfusion-decellularization, whereas native muscle tissue showed its highly structured sarcomere patterns with prominent nuclei. Similar results were obtained by methodological cross-validation of SEM images, which revealed a loss of the strong hierarchy of repetitive sarcomeres in perfusion-decellularized muscle compared to native muscle.

To further support our SHG and SEM image data, we quantified the DNA content per dry muscle tissue in native vs. perfusion-decellularized scaffolds. Our results for native samples, yielding approx. 150 ng mg^{-1} , align well with the

$\sim 120 \text{ ng mg}^{-1}$ DNA content described in literature [34]. In comparison, diffusion-decellularization revealed almost similarly high values of $\sim 140 \text{ ng mg}^{-1}$ and an even higher DNA content for surface tissue, confirming insufficient decellularisation of solid organs when applying diffusion-decellularisation. Perfusion-decellularization however, yielded equally low concentrations for either dynamically strained samples or samples that were held static without external actuation during decellularization.

Both perfusion-decellularization methods fell below the introduced threshold of 50 ng mg^{-1} [28], but were not significantly different from each other. This concludes no negative effect of mechanical actuation on the quality of the decellularized scaffold and therefore, allowed us to implement a further quality parameter to characterize the scaffold, namely: biomechanical assessment of scaffold elasticity through mechanical actuation on-the-fly during the decellularization process.

The data on the scaffold's axial elasticity, obtained from RLT-curves, revealed a marked reduction in maximum restoration force during perfusion-decellularization. Overall, we found passive restoration forces of $\sim 0.35 \text{ N}$ in native *M. gastrocnemius medialis* muscle, that align well with results presented by Jaspers *et al.* (1999) [35], and $\sim 0.25 \text{ N}$ in decellularized muscle scaffolds. When we further approximated the cross-sectional area of $30\text{-}40 \text{ mm}^2$ for *M. gastrocnemius medialis* [36], [37], the elastic modulus of 8.3 kPa aligned well with the lower range reported in literature [38]. In accordance with our findings, Petersen *et al.* (2012) also reported SDS decellularization to reduce passive restoration force in lung tissue [39]. The authors suggested that the detergent diminishes the mechanical integrity of the bio-scaffold via partial loss of native collagen and elastin, eventually leading to a reduced passive mechanical strength [39]. However, Gillies *et al.* (2011) described the ECM as the primary passive load-bearing element [40]. Both proteins contribute largely to ECM composition which is considered to be the primary passive load-bearing element [40], and thus, even a partial loss may result in notable changes in passive stiffness and restoration force. In our study, the overall force reduction calculates to $\sim 30\%$ of the values in native muscle. Apart from contributions of ECM components [40], titin also presents as a key determinant for passive mechanical properties of a muscle and its loss should contribute to a diminished compliance [41], [42]. However, detergent decellularization is known to result in ECM degradation and compromised biomechanical properties [40]. As such, a loss of titin and further elastic components of the ECM likely causes the observed reduction in passive restoration force and renders the decellularized scaffold more compliant in comparison to native muscle tissue. Another aspect includes the irregularly observed swelling of the muscle tissue which also increased scaffold length. Since this phenomenon could not yet be tackled due to a lack of online visual analysis, it was not compensated for and eventually reduced the sample stiffness (or increased compliance), at least to some extent.

While native muscle's axial compliance was centered around 0.015 m N^{-1} , which calculates to a stiffness of $\sim 0.07 \text{ N mm}^{-1}$ and matches with the lower stiffness observed in 200 g Wistar rats ($\sim 0.10 \text{ N mm}^{-1}$) [43], it increased up to $\sim 0.025 \text{ m N}^{-1}$ in

decellularized scaffolds due to a loss of intracellular proteins. Considering that fiber bundles or single fibers are strikingly less affected by highly elastic ECM components [44], it is reasonable for whole muscle to reveal a reduced compliance over fiber bundles or single fibers. Due to a loss of major intracellular elastic proteins, the acellular ECM scaffold still presents stiffer than fiber bundles; yet, more compliant than a native muscle.

V. CONCLUSION

Our engineered *MyoBio* bioreactor system represents a resourceful advancement towards the automated production of skeletal muscle scaffolds for recellularization or reconstructive surgery. Due to its design, it can be applied to various different organs and tissue segments. While we chose a dual perfusion system, the set-up is easily modified into a multi-perfusion bioreactor system. Our automated perfusion-decellularization technique, involving 0.1% SDS, was confirmed to reliably decellularize even deep tissue layers of solid muscle organ and met the quantitative requirements to produce virtually cell-free ECM scaffolds (DNA content $\leq 50 \text{ ng mg}^{-1}$). Since we confirmed mechanical stimulation to not negatively affect decellularization quality, this provided us with the ability to assess the scaffold's passive elasticity in RLT curves online, which will advance to a new process parameter to automatically report the decellularization progress on-the-fly. Therefore, decellularization may no longer be dependent on fixed incubation times, but will rather present as a dynamic process that is dependent on functional and structural parameters. To expand on the latter, we currently strive to implement a 360° optics platform that allows us to measure geometrical parameters (like muscle perimeter, muscle length, muscle shape), and other physical characteristics (like e.g. change in color). Furthermore, we will add a modifiable pressure monitoring system that allows us to measure the internal vascular pressure and the pressure differences to estimate internal leakages and tissue rupture. Future applications as the next step will involve recellularization using stem cell perfusion and adapting cellular supply towards morphological organ parameters monitoring on-the-fly. We believe our bioreactor system represents an important step towards automating TE that provides a universally usable approach to decellularize or modify multiple tissues of interest in a controlled fashion. We expect the system to be a useful advancement for providing new bioartificial tissue constructs for the treatment of VML in reconstructive surgery.

AUTHOR CONTRIBUTIONS STATEMENT

AC, BR, BF, AA and RH provided the animal model and resources. PR, AC, BR, MF, BF, MM, and MH conceptualized and conducted the experiments. PR, MM and KH wrote the software. PR, BR, GP, CL, HS and MH designed and engineered the *MyoBio*. PR, MF, EK, FP and MM performed formal analysis and evaluated the data. AA, RH, OF and MH administered and supervised the project. PR, OF and MH wrote the manuscript. AC, AA, RH, FP, OF and MH acquired funding.

CONFLICT OF INTEREST

The authors declare that there is no conflict of interest.

REFERENCES

- [1] J. Liu, D. Saul, K. O. Böker, J. Ernst, W. Lehman, and A. F. Schilling, "Current methods for skeletal muscle tissue repair and regeneration," *BioMed Res. Int.*, vol. 2018, 2018, Art. no. 1984879.
- [2] C.-H. Lin *et al.*, "Free functioning muscle transfer for lower extremity posttraumatic composite structure and functional defect," *Plast. Reconstructive Surg.*, vol. 119, no. 7, pp. 2118–2126, 2007.
- [3] T. Benjamin, C. L. Corona, H. B. Ward, T. J. B. Walters, and G. J. Christ, "Implantation of in vitro tissue engineered muscle repair constructs and bladder acellular matrices partially restore in vivo skeletal muscle function in a rat model of volumetric muscle loss injury," *Tissue Eng. Part A*, vol. 20, no. 3–4, pp. 705–715, 2014.
- [4] B. Bianchi, C. Copelli, S. Ferrari, A. Ferri, and E. Sesenna, "Free flaps: outcomes and complications in head and neck reconstructions," *J. Cranio-Maxillo-Facial Surg.: Official Pub. Eur. Assoc. Cranio-Maxillo-Facial Surg.*, vol. 37, no. 8, pp. 438–442, 2009.
- [5] "Global observatory on donation and transplantation," Accessed on: Jan. 17, 2022. [Online]. Available: <http://www.transplant-observatory.org>
- [6] A. Masood *et al.*, "A tissue-engineered muscle repair construct for functional restoration of an irrecoverable muscle injury in a murine model," *Tissue Eng. Part A*, vol. 17, no. 17–18, pp. 2291–2303, 2011.
- [7] K. H. Nakayama, M. Shayan, and N. F. Huang, "Engineering biomimetic materials for skeletal muscle repair and regeneration," *Adv. Healthcare Mater.*, vol. 8, no. 5, 2019, Art. no. e1801168.
- [8] K. H. Nakayama *et al.*, "Treatment of volumetric muscle loss in mice using nanofibrillar scaffolds enhances vascular organization and integration," *Commun. Biol.*, vol. 2, 2019, Art. no. 170.
- [9] T. Benjamin *et al.*, "Further development of a tissue engineered muscle repair construct in vitro for enhanced functional recovery following implantation in vivo in a murine model of volumetric muscle loss injury," *Tissue Eng. Part A*, vol. 18, no. 11–12, pp. 1213–1228, 2012.
- [10] M. Juhas, G. C. Engelmayr, A. N. Fontanella, G. M. Palmer, and N. Bursac, "Biomimetic engineered muscle with capacity for vascular integration and functional maturation in vivo," *Proc. Nat. Acad. Sci. United States Amer.*, vol. 111, no. 15, pp. 5508–5513, 2014.
- [11] Y.-J. Choi *et al.*, "3D cell printing of functional skeletal muscle constructs using skeletal muscle-derived bioink," *Adv. Healthcare Mater.*, vol. 5, no. 20, pp. 2636–2645, 2016.
- [12] H. Gregory *et al.*, "Contractile skeletal muscle tissue-engineered on an acellular scaffold," *Plastic Reconstructive Surg.*, vol. 113, no. 2, pp. 595–602, 2004.
- [13] A. Porzionato *et al.*, "Decellularized human skeletal muscle as biologic scaffold for reconstructive surgery," *Int. J. Mol. Sci.*, vol. 16, no. 7, pp. 14808–14831, 2015.
- [14] A. Urciuolo and P. de Coppi, "Decellularized tissue for muscle regeneration," *Int. J. Mol. Sci.*, vol. 19, no. 8, 2018, Art. no. 2392.
- [15] I. T. Ozbolat and Y. Yu, "Bioprinting toward organ fabrication: Challenges and future trends," *IEEE Trans. Biomed. Eng.*, vol. 60, no. 3, pp. 691–699, Mar. 2013.
- [16] D. Ke and S. V. Murphy, "Current challenges of bioprinted tissues toward clinical translation," *Tissue Eng. Part B, Rev.*, vol. 25, no. 1, pp. 1–13, 2019.
- [17] A. N. Leberfinger *et al.*, "Concise review: Bioprinting of stem cells for transplantable tissue fabrication," *STEM CELLS Transl. Med.*, vol. 6, no. 10, pp. 1940–1948, 2017.
- [18] H. C. Ott *et al.*, "Perfusion-decellularized matrix: Using nature's platform to engineer a bioartificial heart," *Nature Med.*, vol. 14, no. 2, pp. 213–221, 2008.
- [19] B. Maher, "How to build a heart," *Nature*, vol. 499, pp. 20–22, 2013.
- [20] S. Sabetkish *et al.*, "Whole-organ tissue engineering: Decellularization and recellularization of three-dimensional matrix liver scaffolds," *J. Biomed. Mater. Res. Part A*, vol. 103, no. 4, pp. 1498–1508, 2015.
- [21] H. C. Ott *et al.*, "Regeneration and orthotopic transplantation of a bioartificial lung," *Nature Med.*, vol. 16, no. 8, pp. 927–933, 2010.
- [22] H. H. Vandenburgh *et al.*, "Skeletal muscle growth is stimulated by intermittent stretch-relaxation in tissue culture," *Amer. J. Physiol.*, vol. 256, no. 3, pp. C674–C682, 1989.
- [23] G. D. Moon, G. Christ, J. D. Stitzel, A. Atala, and J. J. Yoo, "Cyclic mechanical preconditioning improves engineered muscle contraction," *Tissue Eng. Part A*, vol. 14, no. 4, pp. 473–482, 2008.
- [24] B. J. Jank *et al.*, "Engineered composite tissue as a bioartificial limb graft," *Biomaterials*, vol. 61, pp. 246–256, 2015.
- [25] G. D. Mulbauer and W. T. H. Matthew, "Biomimetic scaffolds in skeletal muscle regeneration," *Discoveries*, vol. 7, no. 1, 2019, Art. no. e90.
- [26] B. Perniconi, A. Costa, P. Aulino, L. Teodori, S. Adamo, and D. Coletti, "The pro-myogenic environment provided by whole organ scale acellular scaffolds from skeletal muscle," *Biomaterials*, vol. 32, no. 31, pp. 7870–7882, 2011.
- [27] A. Urciuolo *et al.*, "Decellularised skeletal muscles allow functional muscle regeneration by promoting host cell migration," *Sci. Rep.*, vol. 8, no. 1, 2018, Art. no. 8398.
- [28] M. Peter *et al.*, "An overview of tissue and whole organ decellularization processes," *Biomaterials*, vol. 32, no. 12, pp. 3233–3243, 2011.
- [29] L. J. White *et al.*, "The impact of detergents on the tissue decellularization process: A ToF-SIMS study," *Acta Biomaterialia*, vol. 50, pp. 207–219, 2017.
- [30] R. Simsa *et al.*, "Systematic in vitro comparison of decellularization protocols for blood vessels," *PLoS One*, vol. 13, no. 12, 2018, Art. no. e0209269.
- [31] S. Hinds *et al.*, "The role of extracellular matrix composition in structure and function of bioengineered skeletal muscle," *Biomaterials*, vol. 32, no. 14, pp. 3575–3583, 2011.
- [32] K.-M. Park *et al.*, "Decellularized liver extracellular matrix as promising tools for transplantable bioengineered liver promotes hepatic lineage commitments of induced pluripotent stem cells," *Tissue Eng. Part A*, vol. 22, no. 5–6, pp. 449–460, 2016.
- [33] A. E. Mayorca-Guilliani *et al.*, "Decellularization and antibody staining of mouse tissues to map native extracellular matrix structures in 3D," *Nature Protoc.*, vol. 14, no. 12, pp. 3395–3425, 2019.
- [34] Y. Fu *et al.*, "Decellularization of porcine skeletal muscle extracellular matrix for the formulation of a matrix hydrogel: A preliminary study," *J. Cellular Mol. Med.*, vol. 20, no. 4, pp. 740–749, 2016.
- [35] R. T. Jaspers *et al.*, "Acute effects of intramuscular aponeurotomy on rat gastrocnemius medialis: Force transmission, muscle force and sarcomere length," *J. Biomech.*, vol. 32, no. 1, pp. 71–79, 1999.
- [36] M. Taborowska, D. Bukowska, H. Drzymała-Celichowska, B. Mierzejewska-Krzyżowska, and J. Celichowski, "Morphometric properties and innervation of muscle compartments in rat medial gastrocnemius," *Somatosensory Motor Res.*, vol. 33, no. 3/4, pp. 200–208, 2016.
- [37] Y. F. Heerkens *et al.*, "Mechanical properties of passive rat muscle during sinusoidal stretching," *Eur. J. Physiol.*, vol. 409, no. 4, pp. 438–447, 1987.
- [38] L. Jiang *et al.*, "Correlation between pathological characteristics and Young's modulus value of spastic gastrocnemius in a spinal cord injury rat model," *BioMed Res. Int.*, 2017, 2017, Art. no. 5387948.
- [39] H. Thomas, E. A. Petersen, M. B. C. Colehour, and L. E. Niklason, "Matrix composition and mechanics of decellularized lung scaffolds," *Cells, Tissues, Organs*, vol. 195, no. 3, pp. 222–231, 2012.
- [40] A. R. Gillies *et al.*, "Method for decellularizing skeletal muscle without detergents or proteolytic enzymes," *Tissue Eng. Part C, Methods*, vol. 17, no. 4, pp. 383–389, 2011.
- [41] R. Horowitz, "Passive force generation and titin isoforms in mammalian skeletal muscle," *Biophysical J.*, vol. 61, no. 2, pp. 392–398, 1992.
- [42] J. A. Herzog *et al.*, "Titin (visco-) elasticity in skeletal muscle myofibrils," *Mol. Cellular Biomech.*, vol. 11, no. 1, pp. 1–17, 2014.
- [43] R. D. Woitiez, Y. F. Heerkens, P. A. Huijting, W. H. Rijnsburger, and R. H. Rozendal, "Functional morphology of the m. Gastrocnemius medialis of the rat during growth," *J. Morphol.*, vol. 187, no. 2, pp. 247–258, 1986.
- [44] A. R. Gillies and R. L. Lieber, "Structure and function of the skeletal muscle extracellular matrix," *Muscle Nerve*, vol. 44, no. 3, pp. 318–331, 2011.
- [45] D. Schneiderei *et al.*, "An advanced optical clearing protocol allows label-free detection of tissue necrosis via multiphoton microscopy in injured whole muscle," *Theranostics*, vol. 6, no. 11, pp. 2876–2891, 2021.